

Synthesis, Structure and Properties of the $(\text{Bi}_{0.5}\text{Sr}_{0.5})(\text{Co}_{0.5}\text{Ru}_{0.5})\text{O}_3$ Perovskite

Luis Ortega-San-Martin, Jennifer A. Rodgers, and J. Paul Attfield

Centre for Science at Extreme Conditions (CSEC) and School of Chemistry, University of Edinburgh, King's Buildings, Mayfield Road, EH9 3JZ, Edinburgh, UK

Reprint requests to J. P. Attfield. E-mail: j.p.attfield@ed.ac.uk

Z. Naturforsch. **2008**, *63b*, 641–646; received January 14, 2008

Dedicated to Professor Gérard Demazeau on the occasion of his 65th birthday

The new perovskite $(\text{Bi}_{0.5}\text{Sr}_{0.5})(\text{Co}_{0.5}\text{Ru}_{0.5})\text{O}_3$ has been prepared under high pressure (10 GPa) and temperature (900 °C). The room-temperature crystal structure is described by the space group *Pnma* ($a = 5.5702(3)$, $b = 7.8793(5)$ and $c = 5.5599(4)$ Å) with no observed order between Bi and Sr or between Co and Ru cations. This material shows antiferromagnetic spin ordering or freezing below 50 K and a paramagnetic moment of $4.07 \mu_B$ per formula unit at high temperatures, consistent with the presence of high-spin Co^{2+} or Co^{3+} ions. $(\text{Bi}_{0.5}\text{Sr}_{0.5})(\text{Co}_{0.5}\text{Ru}_{0.5})\text{O}_3$ is a variable range hopping semiconductor between 40 and 300 K with a small negative magnetoresistance.

Key words: Disordered Perovskite, Distorted Perovskite, High-pressure Synthesis, Antiferromagnetism

Introduction

Transition metal oxides of the perovskite-type structure show important physical properties including ferroelectricity and ferromagnetism. These oxides have a general formula ABO_3 with *A* typically being an alkaline, alkaline earth or rare earth cation and *B* often a transition metal [1]. Interesting and useful properties can arise from the coupling of spin, charge and orbital degrees of freedom of the transition metal ions.

When two different ions are ordered on the *B* sites of the perovskite structure, an $\text{A}_2\text{BB}'\text{O}_6$ double perovskite is obtained [2]. The possibility of different degrees of cation order-disorder in these oxides adds another variable that can play an important role in their properties. Oxides of this type have received much attention in recent years due to properties such as large magnetoresistance (*e.g.* $\text{Sr}_2\text{FeMoO}_6$ [3]) and high ionic conductivity in $\text{Sr}_2\text{Mg}_{1-x}\text{Mn}_x\text{MoO}_{6-\delta}$ [4]. Co-existing ferroelectricity and ferromagnetism (multiferroic behaviour) has been reported in $\text{Bi}_2\text{NiMnO}_6$ [5], which may be useful in future electronic devices [6]. In such double perovskites, ferroelectricity can arise from off-centre displacements of a polar cation such as Bi^{3+} or Pb^{2+} in the *A* sites, while magnetic ordering may result from the exchange coupling of the

transition metal cation spins at the *B* sites. However, *B* cations in similar oxidation states (as in the predicted multiferroic $\text{Bi}_2\text{CrFeO}_6$ [7]) are usually disordered [8], and high-temperature and -pressure conditions are needed to stabilize Bi^{3+} in the *A* sites (typically ~ 6 GPa and ~ 1000 °C). Of the phases prepared recently, only $\text{Bi}_2\text{NiMnO}_6$ is cation ordered whereas $\text{BiCo}_{0.5}\text{Mn}_{0.5}\text{O}_3$ [5], $\text{BiCu}_{0.5}\text{Mn}_{0.5}\text{O}_3$ [5] and $\text{BiFe}_{0.5}\text{Cr}_{0.5}\text{O}_3$ [9] show partial or complete disorder and predominantly antiferromagnetic behaviour at low temperatures.

High-pressure and -temperature conditions have been used to prepare new materials since the 1970's but the potential of this synthetic route has only been exploited heavily in the last decade. In the perovskite field, the use of high pressure has led to the discovery of complex *A* and *B* cation orderings, Bi-containing multiferroics, new manganites showing colossal magnetoresistances, and phases with elements in unusual oxidation states [10–12]. Following these previous works, we have attempted the synthesis of the $(\text{BiSr})\text{CoRuO}_6$ double perovskite under high pressure. Substantial Co/Ru *B* site ordering was previously observed in the double perovskites $(\text{LaCa})\text{CoRuO}_6$, $(\text{LaBa})\text{CoRuO}_6$, and $(\text{La}_{1+x}\text{Sr}_{1-x})\text{CoRuO}_6$ ($-0.5 < x < 0.25$) [13, 14].

Experimental Section

The polycrystalline sample was synthesised under high pressure using a Walker-type multianvil apparatus. The precursor was made by a wet-chemical route using a citric acid sol-gel. Stoichiometric quantities of high-purity SrCO_3 , $\text{Co}(\text{CH}_3\text{COO})_2$, Bi_2O_3 and RuO_2 were dissolved in dilute aqueous nitric acid. Citric acid (3 mol per mol of metal) was added to the aqueous solution which was stirred for 1 h to ensure complexation. Ethylene glycol was then added (3/4 mol per mol of citric acid). The solution was dehydrated in a sand bath at 100 °C to a gel which was slowly decomposed in a crucible over one day at 450 °C in air. The resulting mixed oxide powder was ground and calcined several times at temperatures up to 950 °C for 6 h.

~ 20 mg portions of the precursor were transferred to a cylindrical boron nitride crucible at the centre of a pre-cast MgO octahedron, which was compressed to 10 GPa by eight truncated tungsten carbide cubes. A cylindrical graphite resistance heater contacted by two molybdenum plates was used to heat the sample, which was then cooled to ambient temperature before the pressure was released. Approximately 15 mg of an almost phase pure sample were recovered after heating to 900 °C for 15 min. X-Ray powder diffraction confirmed the presence of a perovskite type structure.

Room-temperature X-ray powder diffraction data were collected in the range $15 \leq 2\theta \leq 120^\circ$ with a step size of 0.0069° and an integration time of 2 seconds per step using a Bruker-AXS D8-series-2 X-ray diffractometer with germanium-monochromated $\text{CuK}\alpha$ radiation. The room-temperature crystal structure was analysed by the Rietveld method [15] using the GSAS software package [16].

Magnetic susceptibility measurements were performed using a Quantum Design MPMS-2 SQUID magnetometer whilst heating from 5 to 300 K in an applied field of 10 kOe. Measurements were carried out after field (FC) or zero field (ZFC) coolings. Magnetisation loops between 70 and -70 kOe were measured at 5, 100 and 300 K.

A small pellet of the sample was used for the electrical resistivity measurements on a Quantum Design PPMS system. The data were collected with and without an applied magnetic field of 10 kOe using a 4-probe technique at temperatures from 350 down to 40 K. Below 40 K the sample resistance was too large to be measured. Magnetoresistance in fields up to 80 kOe was measured at 150 and 300 K.

Results

Crystal structure

The X-ray diffraction data show a large number of weak reflections which indicate a significant distortion of the cubic perovskite structure. All peaks were indexed by considering a $\sqrt{2a_p} \times 2a_p \times \sqrt{2a_p}$ expansion

Table 1. Structure refinement results for $(\text{Bi}_{0.5}\text{Sr}_{0.5})\text{Co}_{0.5}\text{Ru}_{0.5}\text{O}_3$ from the Rietveld fit to the room-temperature X-ray diffraction data (space group $Pnma$; $a = 5.5702(3)$, $b = 7.8793(5)$, $c = 5.5599(4)$ Å, $V = 244.02(2)$ Å³, $Z = 4$; overall $U_{\text{iso}} = 0.0078(4)$ Å²; residuals: $R_{\text{wp}} = 3.9\%$, $R_p = 2.9\%$, $R_F^2 = 6.9\%$, $\chi^2 = 1.9\%$).

Atom	Site	x	y	z
Bi/Sr	4c	0.0283(3)	1/4	0.0090(7)
Co/Ru	4b	1/2	0	0
O1	4c	0.003(3)	1/4	0.538(7)
O2	8d	0.281(7)	0.028(4)	0.276(7)

Table 2. Selected bond lengths (Å) and angles (deg) for $(\text{Bi}_{0.5}\text{Sr}_{0.5})(\text{Co}_{0.5}\text{Ru}_{0.5})\text{O}_3$ at $T = 300$ K.

Co/Ru–O1 × 2	1.98(4)	Bi/Sr–O1	2.62(4)
Co/Ru–O2 × 2	1.98(4)	Bi/Sr–O1	2.66(2)
Co/Ru–O2 × 2	2.04(4)	Bi/Sr–O2 × 2	2.69(4)
mean	2.00(4)	Bi/Sr–O2 × 2	2.76(4)
		Bi/Sr–O2 × 2	2.53(3)
		mean	2.66(4)
O1–Co/Ru–O2	93(1)	Co/Ru–O1–Co/Ru	168(1)
O1–Co/Ru–O2	91(2)	Co/Ru–O2–Co/Ru	162(1)
O2–Co/Ru–O2	90(2)		

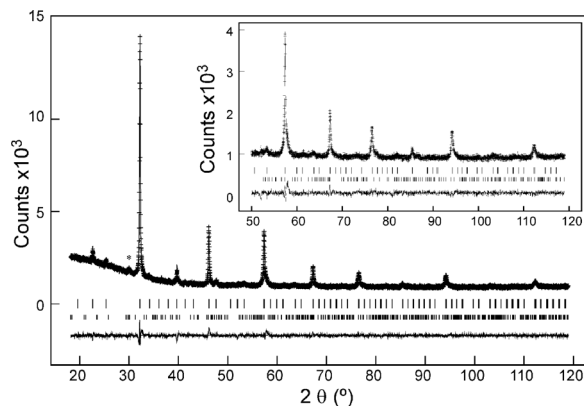
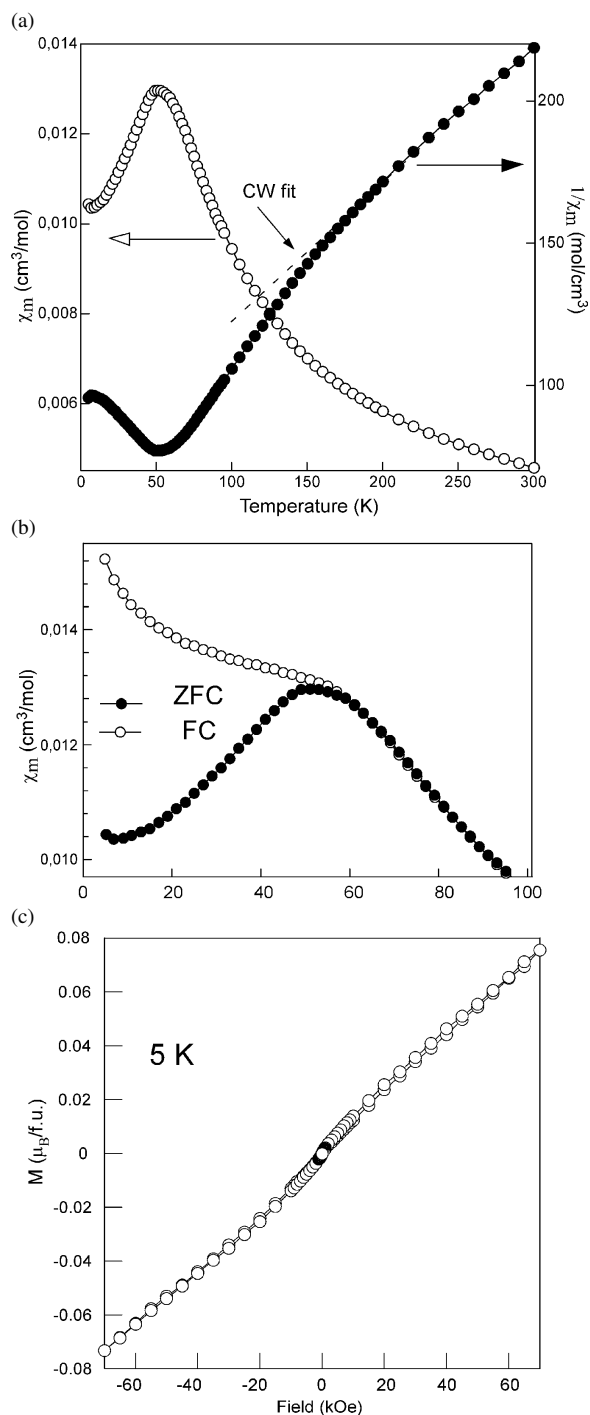


Fig. 1. Rietveld fit to the room-temperature X-ray powder diffraction data of $(\text{Bi}_{0.5}\text{Sr}_{0.5})(\text{Co}_{0.5}\text{Ru}_{0.5})\text{O}_3$ in space group $Pnma$, showing observed, calculated and difference curves. The fit to the high-angle data is inset. Lower tick marks correspond to ~ 1% SrBiO_3 impurity (highest peak indicated as *).

of the cubic lattice using space group $Pnma$ (no. 62). This space group does not describe ordering on the A or B cation sites, showing that the product is the cation-disordered perovskite $(\text{Bi}_{0.5}\text{Sr}_{0.5})(\text{Co}_{0.5}\text{Ru}_{0.5})\text{O}_3$. Attempts to refine the structure in the monoclinic space group $P2_1/n$ which allows B-site ordering confirmed the lack of order so the final refinements were carried out using the $Pnma$ orthorhombic model.

The peak profile was fitted using a modified pseudo-Voigt function, and the background was fitted with a



linear interpolation function. Variable Bi/Sr and oxygen coordinates were refined, and the isotropic displacement parameters of all atoms were constrained to be equal. Final refined parameters and residuals are

← Fig. 2. (a) Temperature dependence of the molar magnetic susceptibility χ_m and the inverse susceptibility for $(\text{Bi}_{0.5}\text{Sr}_{0.5})(\text{Co}_{0.5}\text{Ru}_{0.5})\text{O}_3$ measured at 10 kOe. The dashed line indicates the fit of the Curie-Weiss law. (b) Detail of the low temperature field cooled (FC) and zero field cooled (ZFC) susceptibilities. (c) Magnetisation vs. applied field at 5 K.

given in Table 1, and selected bond lengths and angles are shown in Table 2. The observed, calculated, and difference profiles are shown in Fig. 1.

The crystal structure of $(\text{Bi}_{0.5}\text{Sr}_{0.5})(\text{Co}_{0.5}\text{Ru}_{0.5})\text{O}_3$ is characterised by the tilting of the Co/RuO₆ octahedra along the three axes of the primitive perovskite cell, that can be described as $a^+b^-b^-$, according to the Glazer notation [17]. This changes the Co/Ru–O–Co/Ru angles from the ideal value of 180° to the observed range of 162–168° as shown in Table 2. However, the Co/RuO₆ octahedra remain almost undistorted with internal O–Co/Ru–O angles of 90–93°.

The Co/Ru–O distances show an apparent tetragonal elongation of the Co/RuO₆ octahedra although this is not significant within the error limits. The mean Co/Ru–O distance (Table 2) of 2.00(4) Å is comparable to the expected values for the high-spin Co²⁺–Ru⁵⁺ (2.05 Å), high-spin Co³⁺–low-spin Ru⁴⁺ (2.01 Å) and low-spin Co³⁺–low-spin Ru⁴⁺ (1.97 Å) configurations, but is too imprecise to enable the cation oxidation states to be assigned. The mean Bi/Sr–O distance of 2.66(4) Å is close to the expected value of 2.61 Å. (The calculated distances use published ionic radii [18] assuming 8, 6, and 14/3 coordination numbers for the A, B and O atoms, to allow for the reduced coordination around the A cations in the distorted *Pnma* superstructure).

Magnetic properties

The temperature dependences of the molar magnetic susceptibility χ_m and the inverse susceptibility for $(\text{Bi}_{0.5}\text{Sr}_{0.5})(\text{Co}_{0.5}\text{Ru}_{0.5})\text{O}_3$ are shown in Fig. 2a. At high temperatures (> 160 K) χ_m follows a Curie-Weiss law, $\chi_m = C_m/(T - \theta)$, with $C_m = 2.06 \text{ cm}^3 \cdot \text{K mol}^{-1}$ and $\theta = -150 \text{ K}$, indicating that the predominant exchange interactions are antiferromagnetic. The derived high-temperature paramagnetic moment is $4.07 \mu_B$ per $(\text{Bi}_{0.5}\text{Sr}_{0.5})(\text{Co}_{0.5}\text{Ru}_{0.5})\text{O}_3$ formula unit (f. u.). This value is within the range of 3.9–4.6 μ_B expected for the high-spin Co²⁺–Ru⁵⁺ combination, allowing for a possible orbital contribution to the Co²⁺ moment, but

is also close to the spin-only estimate of $4.0 \mu_B$ for high-spin Co^{3+} -low-spin Ru^{4+} . The low-spin Co^{3+} -low-spin Ru^{4+} combination would have an effective moment of $2.0 \mu_B$ and so is ruled out.

The broad ZFC susceptibility maximum observed for $(\text{Bi}_{0.5}\text{Sr}_{0.5})(\text{Co}_{0.5}\text{Ru}_{0.5})\text{O}_3$ at 50 K shows that antiferromagnetic spin ordering or freezing occurs at low temperatures. The ZFC and FC susceptibilities shown in Fig. 2b diverge below 50 K which could be due to weak ferromagnetism or a spin-glass behaviour. The magnetisation *vs.* applied field loop at 5 K in Fig. 2c shows no significant hysteresis. The slight $H = 0$ offset of the linear M-H relation corresponds to a very small saturated moment of $0.002 \mu_B$ per f. u. which is more likely to be due to a trace of a ferromagnetic impurity such as SrRuO_3 than intrinsic weak ferromagnetism in the main $(\text{Bi}_{0.5}\text{Sr}_{0.5})(\text{Co}_{0.5}\text{Ru}_{0.5})\text{O}_3$ phase. Altogether, the low temperature measurements suggest that at least some glassy character to the spin order is present. Neutron diffraction would be needed to establish clearly whether long-range spin order occurs below ~ 50 K in $(\text{Bi}_{0.5}\text{Sr}_{0.5})(\text{Co}_{0.5}\text{Ru}_{0.5})\text{O}_3$.

Transport properties

The temperature dependence of the electrical resistivity of $(\text{Bi}_{0.5}\text{Sr}_{0.5})(\text{Co}_{0.5}\text{Ru}_{0.5})\text{O}_3$ is shown in Fig. 3. The observed curve is consistent with semiconducting behaviour, and the low temperature data were fitted using the equation (1) derived from the Mott variable-range hopping (VRH) mechanism [19]:

$$\rho = \rho_0 \sqrt{T/T_0} \exp(T_0/T)^{1/(d+1)} \quad (1)$$

where d is the dimensionality of the hopping process and T_0 is the characteristic temperature. The pre-factor is temperature dependent, but is often neglected because of the stronger temperature dependence of the exponential term. The linear variation of $\log \rho$ *vs.* $T^{-1/4}$ (Fig. 3, inset) indicates that a three-dimensional ($d = 3$) VRH process accounts well for the semiconductivity at low temperatures.

The field dependence of the resistivity of $(\text{Bi}_{0.5}\text{Sr}_{0.5})(\text{Co}_{0.5}\text{Ru}_{0.5})\text{O}_3$ was measured at 150 and 300 K. Fig. 4 shows the observed magnetoresistance (MR), calculated as $\text{MR}(H, T) = [\rho(H, T) - \rho(0, T)]/\rho(0, T)$ where H denotes the applied field and $\rho(0, T)$ and $\rho(H, T)$ are the resistivities at zero and H fields, respectively. $\text{Bi}_{0.5}\text{Sr}_{0.5}\text{Co}_{0.5}\text{Ru}_{0.5}\text{O}_3$ shows no significant magnetoresistance at 300 K but a small negative

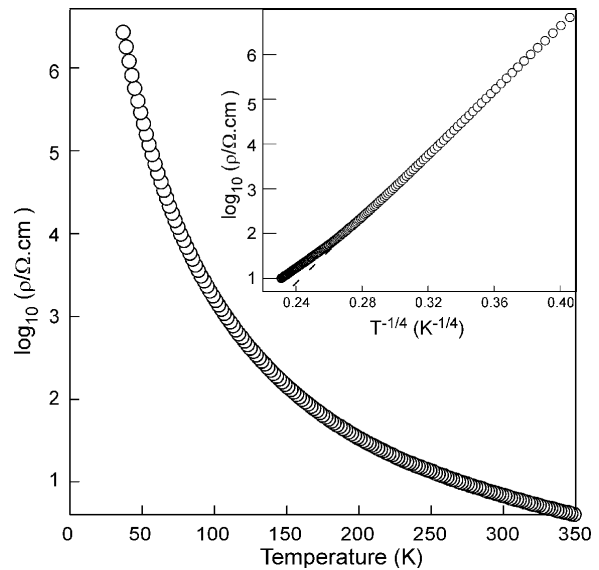


Fig. 3. Temperature dependence of the electrical resistivity for $(\text{Bi}_{0.5}\text{Sr}_{0.5})(\text{Co}_{0.5}\text{Ru}_{0.5})\text{O}_3$. Inset shows the linear low-temperature behaviour of the resistivity as expected from a 3-dimensional VRH model (see text).

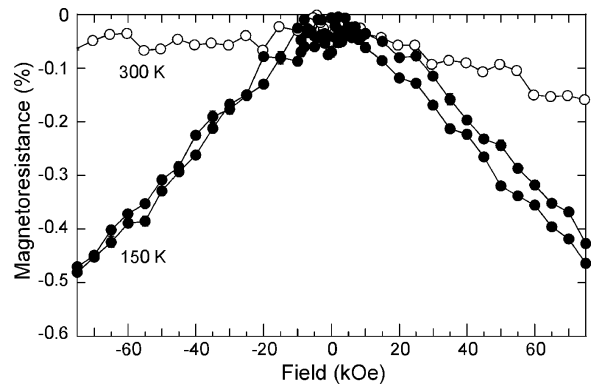


Fig. 4. Field dependence of the magnetoresistance of $(\text{Bi}_{0.5}\text{Sr}_{0.5})(\text{Co}_{0.5}\text{Ru}_{0.5})\text{O}_3$ at 150 and 300 K.

magnetoresistance, up to 0.5 % at 70 kOe, is observed at 150 K.

Discussion

$(\text{Bi}_{0.5}\text{Sr}_{0.5})(\text{Co}_{0.5}\text{Ru}_{0.5})\text{O}_3$ shows a disordered arrangement of Co and Ru over the B sites of an orthorhombic $Pnma$ perovskite structure. The lack of order in this type of complex perovskite shows that there is only a small difference between the oxidation states of the B cations or that they have similar sizes. Similar disorder is found in the phases $\text{SrCo}_{0.5}\text{Ru}_{0.5}\text{O}_3$ [13]

and $\text{La}_{0.5}\text{Sr}_{0.5}\text{Mn}_{0.5}\text{Ru}_{0.5}\text{O}_3$, [20] with $\text{Co}^{3+}\text{-Ru}^{5+}$ and $\text{Mn}^{3+}\text{-Ru}^{4+}$ pairs, respectively. Partial disorder has been claimed for the $M^{2+}\text{-Ru}^{5+}$ pairs in $\text{Ba}_{0.5}\text{-Zn}_{0.5}\text{Ni}_{0.5}\text{Ru}_{0.5}\text{O}_3$ and $\text{Ba}_{0.5}\text{La}_{0.5}\text{Ni}_{0.5}\text{Ru}_{0.5}\text{O}_3$ [21–23], although a high degree of order has been observed in the similar series $(\text{La}_{1-x}\text{Sr}_x)\text{CoRuO}_6$ ($-0.50 \leq x \leq 0.25$), where the $\text{Co}^{2+}\text{-Ru}^{5+}$ combination is observed at $x = 0$ [14]. The greater disruption of the oxygen positions through off-centre distortions of the Bi^{3+} cations in comparison to La^{3+} may suppress long range Co/Ru order in $(\text{Bi}_{0.5}\text{Sr}_{0.5})(\text{Co}_{0.5}\text{Ru}_{0.5})\text{O}_3$. The B-site disorder may also lead to a mixture of $\text{Co}^{2+/3+}$ and $\text{Ru}^{4+/5+}$ states to minimise the Coulombic repulsion energies. Neither the structural nor the magnetic data are able to distinguish between these two limiting configurations, although the magnetic data do demonstrate that the Co ions are in a high-spin state.

The observed structural disorder in $(\text{Bi}_{0.5}\text{Sr}_{0.5})(\text{Co}_{0.5}\text{Ru}_{0.5})\text{O}_3$ leads to a wide range of possible superexchange interactions between the paramagnetic ions and complicates the interpretation of the magnetic data. The predominant interactions are evidently due to antiferromagnetic $M\text{-O-M}$ superexchange, as evidenced by the large negative value of the Weiss temperature, $\theta = -150$ K. The divergence observed between the ZFC and FC curves below the 50 K maximum in the ZFC susceptibility shows that there is a significant glassy component to the spin order. This could be a frozen partial disorder within an antiferromagnetic state, or the ground state of $(\text{Bi}_{0.5}\text{Sr}_{0.5})(\text{Co}_{0.5}\text{Ru}_{0.5})\text{O}_3$

may be a spin glass without any long-range magnetic order.

No resistive anomaly is observed at the 50 K spin freezing or ordering transition, and $(\text{Bi}_{0.5}\text{Sr}_{0.5})(\text{Co}_{0.5}\text{Ru}_{0.5})\text{O}_3$ is semiconducting with 3-dimensional variable range hopping behaviour at low temperatures. A small magnetoresistance is observed in the paramagnetic region, and the linear variation of MR with H shows that it is intrinsic rather than a grain boundary effect. The magnetoresistance may result from local ferromagnetic order and spin-polarised hopping, as is found in several doped cobalt oxides.

In summary, the new phase $(\text{Bi}_{0.5}\text{Sr}_{0.5})(\text{Co}_{0.5}\text{Ru}_{0.5})\text{O}_3$ has been prepared at 10 GPa and 900 °C. It adopts a distorted perovskite-type crystal structure described by the space group $Pnma$ with no observed order between the Co and Ru cations. The B-site charge distribution may be $\text{Co}^{2+}/\text{Ru}^{5+}$ or $\text{Co}^{3+}/\text{Ru}^{4+}$ or intermediate between these two combinations, with Co ions in the high-spin state. Spin ordering or freezing occurs below 50 K. $(\text{Bi}_{0.5}\text{Sr}_{0.5})(\text{Co}_{0.5}\text{Ru}_{0.5})\text{O}_3$ is a variable range hopping semiconductor showing a small negative magnetoresistance.

Acknowledgements

This work has been funded by EPSRC and the Leverhulme Trust. L. Ortega-San-Martin thanks Gobierno Vasco/Eusko Jaurlaritza (Spain) for a Postdoctoral Fellowship. The authors gratefully acknowledge Dr. Javier Sanchez-Benitez for assistance with magnetic and resistivity measurements.

-
- [1] a) J. B. Goodenough, *Rep. Prog. Phys.* **2004**, *67*, 1915–1993; b) F. Galasso, *Perovskites and High Tc superconductors*, Gordon & Breach, New York **1990**.
- [2] R. H. Mitchell, *Perovskites modern and ancient*, Almaz Press, Ontario **2002**.
- [3] K.-I. Kobayashi, T. Kimura, H. Sawada, K. Terakura, Y. Tokura, *Nature* **1998**, *395*, 677–680.
- [4] Y. H. Huang, R. I. Dass, Z.-L. Xing, J. B. Goodenough, *Science* **2006**, *312*, 254–257.
- [5] M. Azuma, K. Takata, T. Saito, S. Ishiwata, Y. Shimakawa, M. Takano, *J. Am. Chem. Soc.* **2005**, *127*, 8889–8892.
- [6] N. A. Spaldin, M. Fiebig, *Science* **2005**, *309*, 391–392.
- [7] P. Baettig, N. A. Spaldin, *Appl. Phys. Lett.* **2005**, *86*, 012505.
- [8] M. T. Anderson, K. B. Greenwood, G. A. Taylor, K. R. Poeppelmeier, *Prog. Solid State Chem.* **1993**, *22*, 197–233.
- [9] M. R. Suchomel, C. I. Thomas, M. Allix, M. J. Rosseinsky, A. M. Fogg, M. F. Thomas, *Appl. Phys. Lett.* **2007**, *90*, 112909. Corrections in *Appl. Phys. Lett.* **2007**, *90*, 209901.
- [10] J. A. Rodgers, A. J. Williams, J. P. Attfield, *Z. Naturforsch.* **2006**, *61b*, 1515–1526.
- [11] S. J. Kim, S. Lemaux, G. Demazeau, J. Y. Kim, J. H. Choy, *J. Am. Chem. Soc.* **2001**, *123*, 10413–10414.
- [12] S. J. Kim, M. J. Martínez-Lope, M. T. Fernández-Díaz, J. A. Alonso, I. Presniakov, G. Demazeau, *Chem. Mater.* **2002**, *14*, 4926–4932.
- [13] S. H. Kim, P. D. Battle, *J. Solid State Chem.* **1995**, *114*, 174–183.
- [14] J. W. G. Bos, J. P. Attfield, *Chem. Mater.* **2004**, *16*, 1822–1827.
- [15] H. M. Rietveld, *J. Appl. Crystallog.* **1969**, *2*, 65.
- [16] A. C. Larson, R. B. Von Dreele, GSAS: General Structure Analysis System, L. AUR 86-748, Los

- Alamos National Laboratory, Los Alamos, NM (USA) **1994**.
- [17] A. M. Glazer, *Acta Crystallogr.* **1975**, *A31*, 756–762; *Acta Crystallogr.* **1972**, *B28*, 3384–3392.
- [18] R. D. Shannon, *Acta Crystallog.* **1976**, *A32*, 751–767.
- [19] N. F. Mott, E. A. Davis, *Electronic Processes in Non-Crystalline Materials*, 2nd ed., Clarendon, Oxford **1979**.
- [20] R. O. Bune, M. V. Lobanov, G. Popov, M. Greenblatt, C. E. Botez, P. W. Stephens, M. Croft, J. Hadermann, G. Van Tendeloo, *Chem. Mater.* **2006**, *18*, 2611–2617.
- [21] K.-P. Hong, Y.-H. Choi, Y.-U. Kwon, D.-Y. Jung, J.-S. Lee, H.-S. Shim, C.-H. Lee, *J. Solid State Chem.* **2000**, *150*, 383–390.
- [22] P. D. Battle, T. C. Gibb, C. W. Jones, F. Studer, *J. Solid State Chem.* **1989**, *78*, 281–293.
- [23] M. Gateshki, J. M. Igartua, *Mater. Res. Bull.* **2003**, *38*, 1893–1900.